

Few-Shot Causal Representation Learning for Out-of-Distribution Generalization on Heterogeneous Graphs

Pengfei Ding

Macquarie University
Sydney, Australia

pengfei.ding2@students.mq.edu.au

Yan Wang

Macquarie University
Sydney, Australia

yan.wang@mq.edu.au

Guanfeng Liu

Macquarie University
Sydney, Australia

guanfeng.liu@mq.edu.au

Nan Wang

Macquarie University
Sydney, Australia

nan.wang12@students.mq.edu.au

Abstract—Heterogeneous graph few-shot learning (HGFL) has been developed to address the label sparsity issue in heterogeneous graphs (HGs), which consist of various types of nodes and edges. The core concept of HGFL is to extract knowledge from rich-labeled classes in a source HG, transfer this knowledge to a target HG to facilitate learning new classes with few-labeled training data, and finally make predictions on unlabeled testing data. Existing methods typically assume that the source HG, training data, and testing data all share the same distribution. However, in practice, distribution shifts among these three types of data are inevitable due to two reasons: (1) the limited availability of the source HG that matches the target HG distribution, and (2) the unpredictable data generation mechanism of the target HG. Such distribution shifts result in ineffective knowledge transfer and poor learning performance in existing methods, thereby leading to a novel problem of out-of-distribution (OOD) generalization in HGFL. To address this challenging problem, we propose a novel Causal OOD Heterogeneous graph Few-shot learning model, namely COHF. In COHF, we first characterize distribution shifts in HGs with a structural causal model, establishing an invariance principle for OOD generalization in HGFL. Then, following this invariance principle, we propose a new variational autoencoder-based heterogeneous graph neural network to mitigate the impact of distribution shifts. Finally, by integrating this network with a novel meta-learning framework, COHF effectively transfers knowledge to the target HG to predict new classes with few-labeled data. Extensive experiments on seven real-world datasets have demonstrated the superior performance of COHF over the state-of-the-art methods.

I. INTRODUCTION

Heterogeneous graphs (HGs), consisting of various types of nodes and edges, have been widely used to model complex real-world systems [1]. For instance, in Fig. 1, there are several HGs that model movie-related social networks. These HGs include different node types such as “movie” and “user”, as well as various edge types, such as “user U_1 likes actor A_5 ” and “director D_4 shoots movie M_{11} ”. The complexity of HGs necessitates substantial labeled data to develop effective models for various HG-related problems (e.g. node classification) [2]. In real-world scenarios, label sparsity is a common issue due to the requirement of expertise and resources to annotate nodes/edges/graphs with specific classes (e.g., classifying “movie” nodes as *family* or *adventure*) [3]. To address this issue, heterogeneous graph few-shot learning

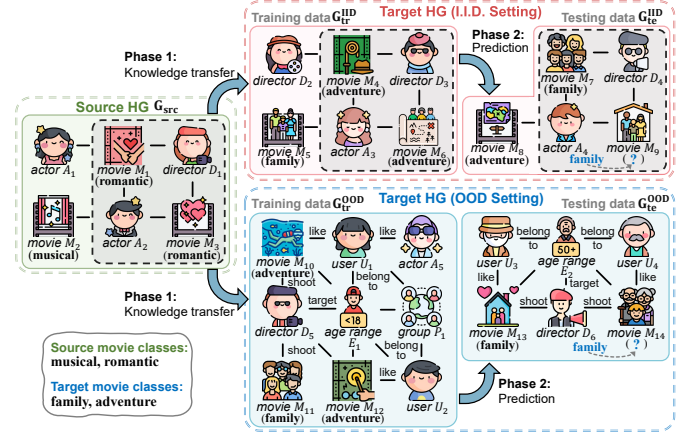


Fig. 1. Heterogeneous graph few-shot scenarios in I.I.D. and OOD settings.

(HGFL) has been developed, which aims to extract generalized knowledge from rich-labeled classes in a source HG, and transfer this knowledge to a target HG to facilitate learning new classes with few-labeled data. The generalized knowledge includes node informativeness [4], heterogeneous information from shared node types [5], and semantic information of specific graph structures [6].

It is worth mentioning that existing HGFL studies generally assume that data is *independently and identically distributed* (I.I.D.), i.e., the rich-labeled data in the source HG, few-labeled training data in the target HG, and unlabeled testing data are all drawn from the same distribution. The reliance on the I.I.D. assumption benefits the simplification of problem modeling and theoretical analysis, which facilitates easier knowledge transfer and HGFL model design [5], [7]. For instance, in Fig. 1, under the I.I.D. setting, the source HG G_{src} , I.I.D. training data $G_{tr}^{I.I.D.}$, and I.I.D. testing data $G_{te}^{I.I.D.}$ are generated from the same distribution, thereby exhibiting similar graph structures and node type distributions, e.g., all three graphs share a common circular structure (outlined by black dashed-line rectangle), where an “actor” node and a “director” node are linked to two “movie” nodes. Specifically, the circular structure in G_{src} includes “actor” A_2 , “director”

D_1 , and “movies” M_1 and M_3 . The fact that both M_1 and M_3 belong to the same class (i.e., *romantic*) reveals knowledge that “movie” nodes in this structure tend to have similar classes. This knowledge can then be transferred to G_{tr}^{IID} . In G_{tr}^{IID} , since “movies” M_4 and M_6 , which are jointly produced by “actor” A_3 and “director” D_3 , also have the same class (i.e., *adventure*), the generalizability of this knowledge can be validated. Consequently, this generalized knowledge can be used to predict the class of “movie” nodes in G_{te}^{IID} , e.g., since M_7 and M_9 are co-produced by “actor” A_4 and “director” D_4 , M_9 is likely to share the same class as M_7 (i.e., *action*).

However, in real-world scenarios, the I.I.D. assumption of existing methods is normally not satisfied. This is mainly because (1) the limited availability of the source HG that perfectly matches the target HG distribution [4], and (2) the unpredictable nature of data generation processes in the target HG [8]. As a result, distribution mismatches (a.k.a. *distribution shifts*) are inevitable between the data in the source HG and the target HG, leading to complex *out-of-distribution* (OOD) environments in HGFL. As a new topic that remains unexplored in the existing literature, OOD environments in HGFL exhibit two unique characteristics as follows:

1. Multi-level Characteristic: Distribution shifts in HGFL can occur at three levels: *feature-level* (e.g., variations in node/edge features), *topology-level* (e.g., changes in graph size or other structural properties), and *heterogeneity-level* (e.g., discrepancies in node/edge types). These different levels of distribution shifts often occur simultaneously. For instance, in Fig. 1, the OOD training data G_{tr}^{OOD} introduces new node types (e.g., “user” and “group”) and new edge types (e.g., “target” and “like”), which are not present in the source HG G_{src} . This leads to a heterogeneity-level shift between G_{src} and G_{tr}^{OOD} . Additionally, these new node and edge types contribute to a different graph structure and an increase in graph size, resulting in a topology-level shift between G_{src} and G_{tr}^{OOD} .

2. Phase-spanning Characteristic: Distribution shifts in HGFL can occur in both the *knowledge transfer* phase and the *prediction* phase of the few-shot learning process. For example, in the OOD setting of Fig. 1, during the knowledge transfer phase, the introduction of new node and edge types in G_{tr}^{OOD} results in a heterogeneity-level shift between G_{src} and G_{tr}^{OOD} . In the prediction phase, the differences in “user age ranges” (i.e., ‘below 18’ vs. ‘over 50’) between G_{tr}^{OOD} and G_{te}^{OOD} lead to variations in “user” node features, yielding a feature-level shift between nodes in these two graphs.

The multi-level and phase-spanning nature of OOD environments in HGFL not only undermines effective knowledge transfer from the source HG to the target HG, but also hinders the adaptation of learned classes from training to testing data. For instance, in Fig. 1, the topology-level shift between G_{src} and G_{tr}^{OOD} makes the circular structure knowledge from G_{src} inapplicable in the OOD setting. Moreover, the feature-level shift between nodes in G_{tr}^{OOD} and G_{te}^{OOD} can lead to incorrect predictions for “movie” nodes in G_{te}^{OOD} . Therefore, it is crucial to investigate the consistency across source HG, training, and testing data, which remains stable in contrast to distribution

shifts. For instance, in Fig. 1, knowledge can be inferred from G_{src} that “movie” nodes connected to the same “director” node typically belong to the same class, such as “movies” M_1 and M_3 linked with “director” D_1 have the same class (*romantic*). This knowledge can be further refined in the OOD setting: “movies” of the same “director” may share a class if they target the same “user” group, e.g., in G_{tr}^{OOD} , “movies” M_{10} and M_{12} directed by D_5 targeting “user” nodes ‘under 18’ fall into the same class (*adventure*). This pattern remains consistent in G_{te}^{OOD} , where “movies” M_{13} and M_{14} directed by D_6 targeting “user” nodes aged ‘over 50’ belong to the same class (*family*). This example illustrates the presence of consistency in OOD environments, and exploring such consistency is important for robust knowledge transfer and accurate predictions.

The above discussion reveals a novel problem of *out-of-distribution generalization on heterogeneous graph few-shot learning*, which aims to handle distribution shifts not only between the source HG and the target HG, but also between the training and testing data in the target HG. To tackle this new problem, we have to face three key challenges as follows.

CH1. *How to figure out the invariance principle in HGs to enable OOD generalization in heterogeneous graph few-shot learning?* The *invariance principle* implies that model predictions, which focus only on the causes of the label, can remain invariant to a range of distribution shifts [9], [10]. This principle forms the cornerstone of many studies that enable OOD generalization in regular Euclidean data (e.g., images) [11]. While recent efforts have extended this principle to non-Euclidean data, addressing distribution shifts in graphs, they primarily focus on homogeneous graphs with a single type of nodes and a single type of edges [12], [13]. However, exploring the invariance principle in heterogeneous graphs is non-trivial, because it requires extracting intricate semantics that remain unaffected by distribution shifts. Such semantics may comprise diverse node and edge types with complicated structural characteristics. Therefore, exploring new invariance principle mechanisms in HGs poses a significant challenge.

CH2. *How to achieve effective knowledge transfer from the source HG to the target HG in OOD environments?* Most HGFL methods transfer knowledge through shared node types and common graph structures between the source HG and the target HG [5], [7]. However, distribution shifts in HGFL can cause heterogeneity and structural variances between these HGs, potentially leading to ineffective knowledge transfer or even negative transfer effects [14]. Therefore, it is crucial to explore a novel framework for effective knowledge transfer in OOD environments. Considering the multi-level nature of distribution shifts within HGs, developing a general knowledge transfer framework is a substantial and complex challenge.

CH3. *Given few-labeled data sampled from an OOD environment, how to effectively learn the class associated with these samples?* Existing few-shot learning methods are primarily designed for I.I.D. environments, with the objective of deriving comprehensive class information from limited samples [15], [16]. However, in OOD environments, it is more effective to focus on aspects of class information that remain invariant with

distribution shifts, rather than attempting to capture all class information. This poses the challenge of identifying invariant class information with only a few labeled samples available.

To address the above three challenges, we propose a novel **Causal OOD Heterogeneous graph Few-shot learning** model, called COHF. To address **CH1**, we construct a structural causal model (SCM) to analyze the cause-effect factors influencing node label generation. By utilizing the SCM, we discover a critical invariance principle for OOD generalization in HGs: heterogeneous graph neural networks (HGNNs) remain invariant to distribution shifts by focusing only on environment-independent factors. To address **CH2**, we follow this principle and propose a novel variational autoencoder-based HGNN module (VAE-HGNN). The VAE-HGNN extracts knowledge about invariant factors from the source HG and transfers it to the target HG, effectively reducing the effects of diverse distribution shifts. To address **CH3**, we propose a novel meta-learning module that transfers the knowledge of measuring the richness of invariant factors from the source HG to the target HG. This module effectively evaluates the importance of few-labeled samples to create robust class representations, thereby enabling accurate predictions on testing data.

To the best of our knowledge, our work is the first to propose the novel problem of OOD generalization in heterogeneous graph few-shot learning and provide a solution for it. Our key contributions are as follows:

- We propose the COHF model, which performs causal modeling and inference to handle various distribution shifts in heterogeneous graph few-shot learning;
- We develop a novel heterogeneous graph neural network module that can extract invariant factors in HGs, and introduce a novel meta-learning module that can achieve effective knowledge transfer and robust predictive performance in OOD environments;
- We conduct extensive experiments on seven real-world datasets. The results demonstrate the superiority of our COHF model over the state-of-the-art methods.

II. RELATED WORK

A. Heterogeneous Graph Representation Learning

Heterogeneous graph representation learning aims to learn low-dimensional node embeddings for various network mining tasks. Recently, heterogeneous graph neural networks (HGNNs) have shown promising results in learning representations on HGs. HGNNs can be categorized into two main groups: type-based and meta-path based. Type-based HGNNs directly model various types of nodes and edges. For example, HetSANN [17] incorporates type-specific graph attention layers to aggregate local information, while Simple-HGN [18] adopts learnable edge type embeddings for edge attention. SlotGAT [19] develops a slot-based message passing mechanism to explore semantics in different node-type feature spaces. In contrast, meta-path based HGNNs focus on modeling meta-paths to extract hybrid semantics in HGs. For instance, HAN [20] employs a hierarchical attention

mechanism to capture node-level importance between nodes and semantic-level importance of meta-paths. MAGNN [21] provides an advanced approach with several meta-path encoders to encode comprehensive information along meta-paths. GTN [22] can automatically learn meta-paths using graph transformation layers. However, these methods often assume the same distribution between training and testing data, which limits their generalizability to OOD environments in HGs.

B. Graph Few-shot Learning

Graph few-shot learning combines few-shot learning with GNNs to address label sparsity issues. Most existing studies focus on homogeneous graphs [2]. For example, Meta-GNN [23] combines GNNs with the MAML algorithm [15] for effective graph learner initialization. G-Meta [16] utilizes meta-gradients from local subgraphs to update network parameters. Recent studies have extended few-shot learning to heterogeneous graphs. For instance, HINFSHOT [5] focuses on few-shot problems within a single citation network. CrossHG-Meta [24] and HG-Meta [7] leverage shared meta-paths between source and target HGs for enhanced generalizability. However, these methods overlook distribution shifts in HGs, which can hinder knowledge transfer and reduce the prediction performance. CGFL [4] addresses the cross-heterogeneity challenge by simplifying heterogeneous information into two general patterns for knowledge transfer. However, this approach still overlooks distribution shifts between training and testing data. Additionally, this simplification may lead to the loss of specific node type information, limiting the capability to capture invariant heterogeneous information in OOD environments.

C. OOD Generalization on Graphs

Some pioneering works [25], [26] have investigated whether models trained on small graphs can generalize effectively to larger ones [27]. Recently, researchers have extended OOD generalization methods, such as the invariance principle [28], to explore graph structures that are resilient to distribution shifts. For instance, DIR [29] divides a graph into causal and non-causal components using an edge threshold. CIGA [12] aims to maximize the agreement between the invariant portions of graphs with the same labels. CAL [30] uncovers causal patterns and mitigates the confounding effects of shortcuts. DisC [13] investigates learning causal substructures in scenarios with severe bias. However, most of these efforts focus on graph classification tasks in homogeneous graphs. Notably, there is a lack of research addressing more comprehensive graph distribution shifts in heterogeneous graphs.

III. PRELIMINARIES

Heterogeneous Graph. A heterogeneous graph is defined as $G = (\mathcal{V}, \mathcal{E}, \mathcal{S}_n, \mathcal{S}_e)$, where \mathcal{V} represents the set of nodes with a node type mapping function $\varphi(v) : \mathcal{V} \mapsto \mathcal{S}_n$, and \mathcal{E} denotes the set of edges with an edge type mapping function $\psi(e) : \mathcal{E} \mapsto \mathcal{S}_e$. Here, \mathcal{S}_n and \mathcal{S}_e represent the sets of node types and edge types, respectively. Each node $v \in \mathcal{V}$ or edge $e \in \mathcal{E}$ is associated with a specific type. Note that for heterogeneous

TABLE I
NOTATIONS USED IN THIS PAPER.

Notation	Explanation
G	Heterogeneous graph
\mathcal{V}	Set of nodes
$\varphi(\cdot)$	Node type mapping function
Φ	Single node type
\mathcal{S}_n	Set of node types
$\tau = (\tau_{spt}, \tau_{qry})$	Single few-shot task
$p_\theta(\cdot)$	Distribution parameterized by θ
$q_\phi(\cdot)$	Variational distribution parameterized by ϕ
rel^c	Set of common relations
rel^u	Set of unique relations
a_{uv}	Connectivity between nodes u and v
A	Adjacency matrix
G_s	Subgraph structure around the target node
\mathbf{X}	Raw node features
$\mathbf{H}^{(l)}$	Hidden embedding of the l -th layer
\mathbf{h}_v	Hidden embedding of node v
\mathbf{W}	Weight matrix
α, γ	Normalized attention weight
$\text{rsl}(\cdot), \text{rnl}(\cdot)$	Richness score of structure-level and node-level
proto_c	Prototype embedding of class c

graphs, $|\mathcal{S}_n| + |\mathcal{S}_e|$ should be greater than 2. Table I summarizes frequently used notations in this paper for quick reference.

Problem Formulation. We focus on the problem of few-shot node classification in HGs under OOD environments. To mimic the few-shot scenario, we create two sets of few-shot tasks for the source and target HGs, named as \mathcal{T}_{src} for the source HG and \mathcal{T}_{tgt} for the target HG.

- **Input:** Source HG G_{src} with its few-shot task set \mathcal{T}_{src} . Target HG training data G_{tgt}^{tr} with its few-shot task set \mathcal{T}_{tgt} , where the distribution $\Psi(G_{src}) \neq \Psi(G_{tgt}^{tr})$.
- **Output:** A model with good generalization ability to accurately predict the labels of nodes in the target HG testing data G_{tgt}^{te} , where the distribution $\Psi(G_{tgt}^{tr}) \neq \Psi(G_{tgt}^{te})$.

Few-shot Task Construction. The set of m few-shot tasks, denoted as $\mathcal{T} = \{\tau_1, \tau_2, \dots, \tau_m\}$, is constructed for both the source HG and the target HG as follows: Under the N -way K -shot setting, each task $\tau = (\tau_{spt}, \tau_{qry})$ is composed by first selecting N different classes $C_\tau = \{c_1, c_2, \dots, c_N\}$ from the label space C . Then, the support set $\tau_{spt} = \{\tau_{c_1}, \tau_{c_2}, \dots, \tau_{c_N}\}$ is formed by sampling K labeled nodes from each class, i.e., $\tau_{c_i} = \{(v_1, c_i), (v_2, c_i), \dots, (v_K, c_i)\}$. The query set $\tau_{qry} = \{\tilde{\tau}_{c_1}, \tilde{\tau}_{c_2}, \dots, \tilde{\tau}_{c_N}\}$ is created using the remaining data from each class, where $\tilde{\tau}_{c_i} = \{(\tilde{v}_1, c_i), (\tilde{v}_2, c_i), \dots, (\tilde{v}_K, c_i)\}$.

For each target HG few-shot task $\tau \in \mathcal{T}_{tgt}$, the support set and query set are sampled from the training data G_{tgt}^{tr} and the testing data G_{tgt}^{te} , respectively. After completing sufficient training iterations over all few-shot tasks in the source HG (\mathcal{T}_{src}), the obtained model is expected to solve each few-shot task in the target HG (\mathcal{T}_{tgt}) by performing N -way classification in G_{tgt}^{te} , utilizing only K labeled examples per class from G_{tgt}^{tr} .

IV. INVARIANCE PRINCIPLE FOR OOD GENERALIZATION ON HETEROGENEOUS GRAPHS

In this section, we first explore the label generation process in HGs from a causal perspective and introduce a novel

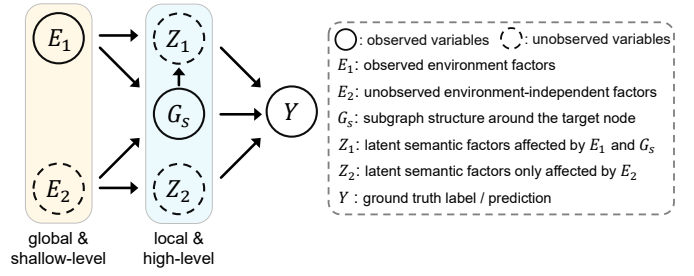


Fig. 2. Structure causal model (SCM) for node label generation in HGs.

structural causal model (SCM) to conceptualize this process. Next, we leverage this SCM to investigate the invariance principle in HGs. This principle serves as the foundation for enabling OOD generalization in HGFL.

A. Causal Perspective on Node Label Generation

Considering a target node v_t in an HG G , we adopt a causal perspective on the label generation process of v_t and construct an SCM, as illustrated in Fig. 2. The rationale behind this SCM is explained as follows:

- E_1 and E_2 represent the global information of G :
 E_1 includes the overall graph structure, along with the input features of the nodes and edges in G . We consider that these observable factors are shaped by the underlying environmental context behind the HG. Different contexts can result in variations in the graph's structure and the unique features of its nodes and edges, leading to distribution shifts across HGs. For instance, in social networks, when diverse social communities (e.g., students, professionals, and celebrities) are modeled as HGs, they exhibit distinct node/edge types, features, and connection patterns.
 E_2 represents factors that are consistent regardless of environmental changes, i.e., *environment-independent* factors. These factors are typically elusive and not directly observable, such as the uniformity of user behaviors across different social networks and the general tendencies of consumers to follow purchasing trends in e-commerce networks. Both E_1 and E_2 include node-level and edge-level features but lack compound semantic information, making them global yet shallow in nature.
- Z_1 and Z_2 represent the semantic information associated with the target node v_t . Z_1 includes semantic factors influenced by global environment factors E_1 , while Z_2 represents those unaffected by E_1 . In the node label generation process, these factors are intricate semantic information related to v_t , making them local yet high-level in nature.
- G_s denotes the subgraph structure comprising v_t and its neighbors. This subgraph structure can be extracted using methods like considering the k -hop neighbors of v_t in G . Therefore, G_s is an observable variable.
- Y denotes the category or label assigned to v_t .
- $(E_1, E_2) \rightarrow G_s$ indicates that on the one hand, the subgraph G_s is extracted from G and thus is influenced by environmental factors E_1 . On the other hand, existing research has

revealed the consistency of node connections across various environments [4], [31], [32]. This implies that G_s is also shaped by environment-independent factors E_2 .

- $(E_1, G_s) \rightarrow Z_1$ and $E_2 \rightarrow Z_2$ suggest that the high-level semantic factors are derived from combinations of shallow-level factors. These semantic factors, Z_1 and Z_2 , are unobservable and typically require domain-specific knowledge for identification. For instance, researchers often utilize pre-defined meta-paths [33] and meta-graphs [34] that consist of diverse node types to extract semantic information. Specifically, Z_1 is determined by both the global environment factors E_1 and the subgraph G_s , while Z_2 is independent of the environment and does not depend on G_s .
- $(Z_1, Z_2, G_s) \rightarrow Y$ means that the label of v_t depends on the high-level semantic factors and the subgraph.

Connection with Existing Works and Novel Insights. While introducing the SCM for node label generation in HGs for the first time, we observe that the SCM’s causal relations not only align with established paradigms in existing literature, but also provide fresh and unique perspectives, as outlined below:

- **Capturing semantic information in HGs from shallow to high levels:** Since directly capturing complex semantic information within HGs is challenging [35], existing methods typically adopt a hierarchical learning approach, leveraging diverse node types to capture complex heterogeneous information and reveal underlying semantics [20], [21]. Differently, our SCM extends this approach by focusing on the capture of semantic information in OOD environments. It combines shallow-level factors to obtain environmental semantic factors and invariant semantic factors.
- **Leveraging semantic information for node labeling:** Investigating node-related semantic information is crucial for accurate node classification [36], [37]. Existing methods tend to focus on explicit semantic information within individual HGs. In contrast, our SCM highlights the importance of invariant implicit semantic information across various HGs, providing a new perspective on node labeling.
- **Extracting semantic factors from subgraphs:** Previous studies indicate that local subgraphs can retain substantial node-related properties for node-level tasks [16], [38]. Focusing on local subgraphs also improves model scalability and generalizability [39], [40]. Unlike these studies, our SCM advances this concept by exploring the connection between subgraphs and global factors. It aims to identify unobservable, environment-independent factors in the subgraph generation process, thereby enhancing the understanding of semantic factor extraction.

B. Exploring Invariance for OOD Generalization on HGs

We first analyze how distribution shifts occur in HGs and formulate OOD generalization from a causal perspective. Then, we propose the invariance principle, which focuses on leveraging invariant factors through distribution shifts to address OOD generalization problems.

In the SCM depicted in Fig. 2, a distribution shift occurs when there are changes in observed factors. Specifically, this

shift happens if the global environment factors E_1 and/or the subgraph of the target node G_s change. We particularly focus on scenarios where both E_1 and G_s change simultaneously. Such scenarios are highly relevant for OOD environments in HGFL, because both E_1 and G_s concurrently undergo changes during knowledge transfer and prediction phases. To elaborate on the distribution shifts between two HGs, we denote E_1 and G_s in one HG as \mathbf{e}_1 and \mathbf{g} , respectively, and in another HG as \mathbf{e}'_1 and \mathbf{g}' . From a causal view, the distribution shift from $(E_1 = \mathbf{e}_1, G_s = \mathbf{g})$ to $(E_1 = \mathbf{e}'_1, G_s = \mathbf{g}')$ is formulated as an *intervention* [41], denoted as $do(E_1 = \mathbf{e}'_1, G_s = \mathbf{g}')$. Therefore, OOD generalization in HGs can be modeled as a *post-intervention inference* of node label probabilities $P(Y|do(E_1 = \mathbf{e}'_1, G_s = \mathbf{g}'), \mathbf{e}_2)$, where \mathbf{e}_2 represents the factors of E_2 that remain unchanged during the distribution shift.

Considering that the intervention $do(E_1 = \mathbf{e}'_1, G_s = \mathbf{g}')$ only affects Z_1 , we can leverage the unaffected factors, E_2 and Z_2 , to facilitate generalization between HGs with distribution shifts. Therefore, the invariance principle for OOD generalization in HGs is that *models are invariant to distribution shifts if they focus only on the environment-independent factors E_2 and latent semantic factors Z_2* . While E_2 and Z_2 are unobservable, Z_2 can be inferred from E_2 , as it is only determined by E_2 . Thus, the main challenge is to acquire E_2 . We will introduce a method to address this challenge in the next section.

V. METHODOLOGY

A. Overview

In this section, we introduce our Causal OOD Heterogeneous graph Few-shot learning model, named COHF. The core concept of COHF is utilizing invariant factors within HGs to facilitate knowledge transfer and class learning with few-labeled data in OOD environments. (1) For effective knowledge transfer, COHF proposes a variational autoencoder-based HGNN (VAE-HGNN). VAE-HGNN first models causal relations within the SCM and then applies causal inference on these relations to identify invariant factors that remain unaffected by distribution shifts. By integrating this VAE-HGNN with a meta-learning framework, the knowledge of these invariant factors can be transferred from the source HG to the target HG. (2) To ensure stable class learning from few-labeled samples, COHF evaluates the richness of invariant factors in each sample. Specifically, by assessing invariant factors at both the structural and node levels, COHF prioritizes samples with rich invariant factors, thereby capturing class information that remains stable despite distribution shifts. Overall, by exploring and utilizing invariant factors in both the knowledge transfer and class learning processes, COHF effectively handles OOD environments in heterogeneous graph few-shot learning.

B. Variational Autoencoder-based HGNN

Fig. 3 illustrates the architecture of VAE-HGNN, which is closely aligned with the structure of our proposed SCM. For the three unobservable variables in the SCM, *i.e.*, the environment-independent factors E_2 , and the latent semantic

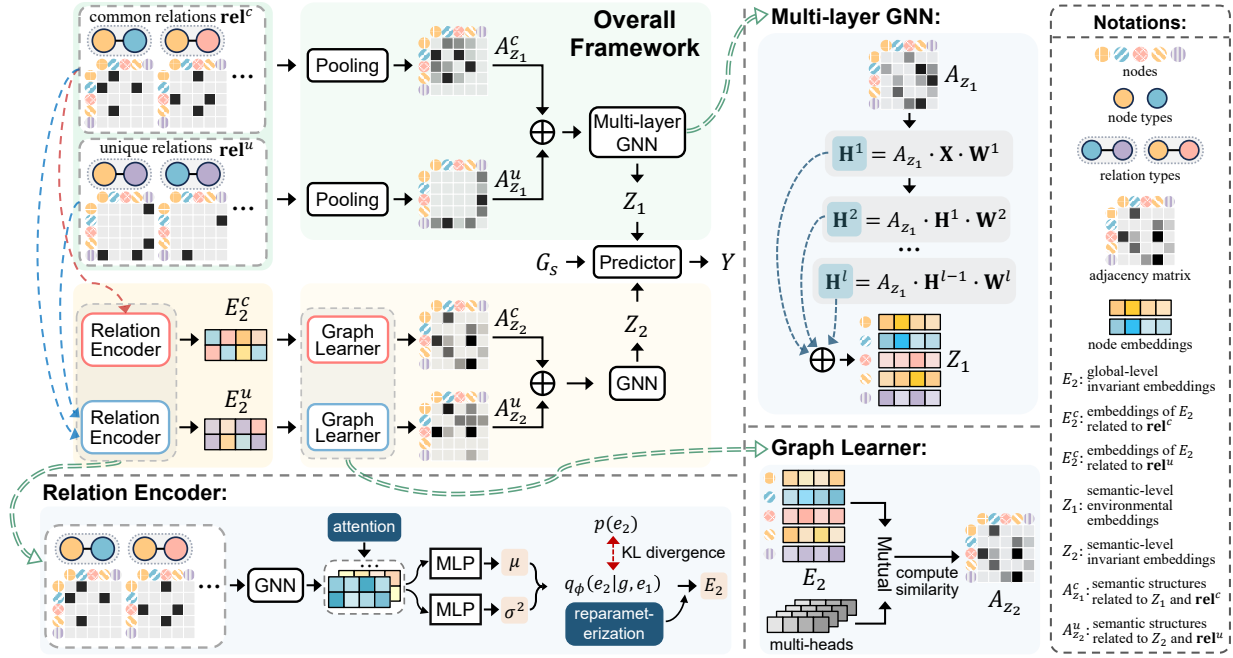


Fig. 3. The overall architecture of VAE-HGNN.

factors Z_1 and Z_2 , we propose three modules to model each of these variables: (1) The *relation encoder* module infers E_2 by leveraging the observed global information and subgraph structure. (2) The *multi-layer GNN* module infers Z_1 based on global heterogeneous information E_1 and the subgraph structure G_s . (3) The *graph learner* module infers Z_2 using E_2 , where E_2 is deduced by the relation encoder module. Overall, this framework can be viewed as a combination of an encoder, which utilizes the relation encoder to infer E_2 , and a decoder that employs E_1 , E_2 , and G_s to predict the label Y .

Causal Inference for OOD Generalization in HGs. Before a distribution shift occurs, we assume all observed variables as ($E_1 = \mathbf{e}_1$, $G_s = \mathbf{g}$, $Y = \mathbf{y}$). Since the environment-independent factor $E_2 = \mathbf{e}_2$ remains invariant to distribution shifts, our goal is to infer \mathbf{e}_2 conditional on these observed variables, *i.e.*, the posterior distribution $p_\theta(\mathbf{e}_2|\mathbf{y}, \mathbf{e}_1, \mathbf{g})$ that is parameterized by θ . However, this distribution is usually intractable due to the complexity of the joint distribution $p(\mathbf{y}, \mathbf{e}_1, \mathbf{g})$. To tackle this challenge, we resort to variational inference [42], [43] and introduce a variational distribution $q_\phi(\mathbf{e}_2|\mathbf{y}, \mathbf{e}_1, \mathbf{g})$, parameterized by ϕ , to approximate the true posterior $p_\theta(\mathbf{e}_2|\mathbf{y}, \mathbf{e}_1, \mathbf{g})$.

Learning Objective. Following the VAE mechanism in [43], [44], we train the model parameters θ and ϕ by optimizing the Evidence Lower Bound (ELBO), which is a lower bound for the log-likelihood of $p_\theta(\mathbf{y}|\mathbf{g}, \mathbf{e}_1)$. Here, $p_\theta(\mathbf{y}|\mathbf{g}, \mathbf{e}_1)$ is the probability of the desired label $Y = \mathbf{y}$ conditioned on the observable global environment factors $E_1 = \mathbf{e}_1$ and subgraph $G_s = \mathbf{g}$. The negative ELBO loss \mathcal{L}_{ELBO} is defined as follows:

$$\begin{aligned} \log p_\theta(\mathbf{y}|\mathbf{g}, \mathbf{e}_1) &\geq \mathbb{E}_{q_\phi(\mathbf{e}_2|\mathbf{y}, \mathbf{g}, \mathbf{e}_1)} [\log p_\theta(\mathbf{y}|\mathbf{g}, \mathbf{e}_1, \mathbf{e}_2)] - \\ &\quad KL[q_\phi(\mathbf{e}_2|\mathbf{y}, \mathbf{g}, \mathbf{e}_1)||p(\mathbf{e}_2)] \\ &\triangleq -\mathcal{L}_{ELBO}. \end{aligned} \quad (1)$$

Proof (We abbreviate $\mathbb{E}_{q_\phi(\mathbf{e}_2|\mathbf{y}, \mathbf{g}, \mathbf{e}_1)}$ as \mathbb{E}_{q_ϕ} for simplicity).

$$\begin{aligned} &\log p_\theta(\mathbf{y}|\mathbf{g}, \mathbf{e}_1) \\ &= \log \left(\mathbb{E}_{q_\phi} \left[\log \frac{p_\theta(\mathbf{y}|\mathbf{g}, \mathbf{e}_1)}{q_\phi(\mathbf{e}_2|\mathbf{y}, \mathbf{g}, \mathbf{e}_1)} \right] \right) \\ &\geq \mathbb{E}_{q_\phi} \left[\log \frac{p_\theta(\mathbf{y}|\mathbf{g}, \mathbf{e}_1)}{q_\phi(\mathbf{e}_2|\mathbf{y}, \mathbf{g}, \mathbf{e}_1)} \right] \\ &= \mathbb{E}_{q_\phi} [\log p_\theta(\mathbf{y}|\mathbf{g}, \mathbf{e}_1)] - \mathbb{E}_{q_\phi} [\log q_\phi(\mathbf{e}_2|\mathbf{y}, \mathbf{g}, \mathbf{e}_1)] \\ &= \mathbb{E}_{q_\phi} [\log p_\theta(\mathbf{y}|\mathbf{g}, \mathbf{e}_1, \mathbf{e}_2)p(\mathbf{e}_2)] - \mathbb{E}_{q_\phi} [\log q_\phi(\mathbf{e}_2|\mathbf{y}, \mathbf{g}, \mathbf{e}_1)] \\ &= \mathbb{E}_{q_\phi} [\log p_\theta(\mathbf{y}|\mathbf{g}, \mathbf{e}_1, \mathbf{e}_2)] - \mathbb{E}_{q_\phi} \left[\log \frac{q_\phi(\mathbf{e}_2|\mathbf{y}, \mathbf{g}, \mathbf{e}_1)}{p(\mathbf{e}_2)} \right] \\ &= \mathbb{E}_{q_\phi} [\log p_\theta(\mathbf{y}|\mathbf{g}, \mathbf{e}_1, \mathbf{e}_2)] - KL[q_\phi(\mathbf{e}_2|\mathbf{y}, \mathbf{g}, \mathbf{e}_1)||p(\mathbf{e}_2)]. \quad \square \end{aligned}$$

In Eq. (1), the first term accounts for label regeneration, while the second term regularizes the Kullback-Leibler (KL) divergence between $q_\phi(\mathbf{e}_2|\mathbf{y}, \mathbf{g}, \mathbf{e}_1)$ and $p(\mathbf{e}_2)$. We assume \mathbf{e}_2 is a D -dimension latent vector sampled from a standard Gaussian prior [45], *i.e.*, $p(\mathbf{e}_2) = \mathcal{N}(0, I_D)$. The rationale behind Eq. (1) is that minimizing the ELBO loss \mathcal{L}_{ELBO} corresponds to maximizing the log-likelihood of the observed data $\log p_\theta(\mathbf{y}|\mathbf{g}, \mathbf{e}_1)$. To compute \mathcal{L}_{ELBO} , we design an encoder and a decoder, each consisting of several modules, to model $q_\phi(\mathbf{e}_2|\mathbf{y}, \mathbf{g}, \mathbf{e}_1)$ and $p_\theta(\mathbf{y}|\mathbf{g}, \mathbf{e}_1, \mathbf{e}_2)$, respectively.

Encoder. To infer the invariant factor $E_2 = \mathbf{e}_2$ with the posterior distribution $q_\phi(\mathbf{e}_2|\mathbf{y}, \mathbf{g}, \mathbf{e}_1)$, we first approximate $q_\phi(\mathbf{e}_2|\mathbf{y}, \mathbf{g}, \mathbf{e}_1)$ as $q_\phi(\mathbf{e}_2|\mathbf{g}, \mathbf{e}_1)$. This approximation, known as the mean-field method, is commonly used in variational inference based methods [46]. Inspired by variational autoencoders [43], we define $q_\phi(\mathbf{e}_2|\mathbf{g}, \mathbf{e}_1)$ as a multivariate Gaussian with a diagonal covariance structure, which is flexible and allows \mathcal{L}_{ELBO} to be computed analytically [45]. Accordingly,

the encoder is designed as follows:

$$\mathbf{h} = g_\phi(\mathbf{g}, \mathbf{e}_1), \quad (2)$$

$$q_\phi(\mathbf{e}_2|\mathbf{g}, \mathbf{e}_1) = \mathcal{N}(\mu_\phi(\mathbf{h}), \sigma_\phi^2(\mathbf{h})\mathbf{I}), \quad (3)$$

where $g_\phi(\cdot)$ is a GNN-based module to capture graph structure information. $\mu_\phi(\cdot)$ and $\sigma_\phi^2(\cdot)$ are multi-layer perceptrons (MLPs) that convert \mathbf{h} into the mean and standard deviations, which parameterize the distribution of $q_\phi(\mathbf{e}_2|\mathbf{g}, \mathbf{e}_1)$. Since $q_\phi(\mathbf{e}_2|\mathbf{g}, \mathbf{e}_1)$ takes on a Gaussian form, the reparameterization trick from variational autoencoders [43] can be employed here to calculate the derivatives *w.r.t.* the encoder parameters.

The neural network architecture of $g_\phi(\cdot)$ should be designed according to specific practical scenarios. For our target OOD environments in HGFL, the goal is to ensure effective knowledge transfer when distribution shifts occur at three distinct levels: feature-level, topology-level, and heterogeneity-level. Accordingly, we have the following design considerations.

- Considering feature-level shifts, we define E_2 as invariant node-level feature representations. This ensures that $g_\phi(\cdot)$ generates consistent node representations despite input features undergo various feature-level shifts.
- Considering topology-level shifts, we aim to learn features that are independent of the specific graph structures or patterns. To this end, we focus on capturing relation-level information between nodes, which is not reliant on particular graph structures or patterns [32].
- Considering heterogeneity-level shifts between two HGs G_1 and G_2 , differing node types lead to a variety of relation types. We categorize these relation types into two sets: \mathbf{rel}^c that includes common relation types in both HGs, and \mathbf{rel}^u that contains unique relation types for each HG. Formally, $\mathbf{rel}^c = \{(\Phi_i, \Phi_j) | (\Phi_i, \Phi_j) \in \mathcal{S}_n^1, (\Phi_i, \Phi_j) \in \mathcal{S}_n^2\}$, where Φ_i and Φ_j are two node types in G_1 and G_2 , and \mathcal{S}_n^1 and \mathcal{S}_n^2 are the node type sets of G_1 and G_2 , respectively. Note that only node types (Φ_i, Φ_j) with connections in both G_1 and G_2 are considered. $\mathbf{rel}_1^u = \{(\Phi_i, \Phi_j) | (\Phi_i, \Phi_j) \in \mathcal{S}_n^1, (\Phi_i, \Phi_j) \notin \mathcal{S}_n^2\}$ is the unique relation set in G_1 . Thus, a heterogeneity-level shift from $E_1 = \mathbf{e}_1$ to $E_1 = \mathbf{e}_1'$ implies that $\mathbf{rel}^c(\mathbf{e}_1) = \mathbf{rel}^c(\mathbf{e}_1')$, while $\mathbf{rel}^u(\mathbf{e}_1) \cap \mathbf{rel}^u(\mathbf{e}_1') = \emptyset$.
- Considering the effectiveness of knowledge transfer between HGs with significant structural and size differences, we aim to capture generalized structural knowledge by focusing on similar subgraph structures, rather than the entire HG. Specifically, we extract subgraphs from n_k -hop neighbors to create similarly scaled G_s across HGs with varying sizes.

Based on the above analysis, we propose two subgraph-based relation encoders to learn invariant node-level feature representations from common relations \mathbf{rel}^c and unique relations \mathbf{rel}^u , respectively. Given all node features $\mathbf{X} = \{\mathbf{x}_v | v \in \mathcal{V}_s\}$ and subgraph G_s , where \mathcal{V}_s is the set of nodes in G_s , the inputs for these two modules are the adjacency matrices of \mathbf{rel}^c and \mathbf{rel}^u in G_s , denoted as \mathbf{A}^c and \mathbf{A}^u , respectively. For instance, $\mathbf{A}^c = \{A_{i,j} | (\Phi_i, \Phi_j) \in \mathbf{rel}^c\}$, where the adjacency matrix $A_{i,j} = \{a_{mn} | m, n \in \mathcal{V}_s, \varphi(m) = \Phi_i, \varphi(n) = \Phi_j\}$, here a_{mn} is the connectivity between nodes m and n .

The rationale behind the relation encoders lies in our assumption that both common relations \mathbf{rel}^c and unique relations \mathbf{rel}^u contain features that remain unaffected by distribution shifts. For \mathbf{rel}^c , these invariant features are inherent within the relations themselves. In contrast, for \mathbf{rel}^u , the invariant features arise from the interactions between \mathbf{rel}^c and \mathbf{rel}^u . These interactions essentially reflect how common relations interact with those that are susceptible to distribution shifts. Therefore, we design two relation encoders to capture these two types of invariant features. Specifically, for the common relation encoder, we first employ a GNN to learn the representation of a node v under the i -th relation type $r_i \in \mathbf{rel}^c$ as follows:

$$\mathbf{h}_{v-i}^c = \text{GNN}_c(A_i^c, \mathbf{x}_v), \quad (4)$$

where $A_i^c \in \mathbf{A}^c$ is the adjacency matrix of r_i . Then, we adopt an attention mechanism to aggregate information from different relation types in \mathbf{rel}^c as follows:

$$\alpha_{v-i}^c = \frac{\exp(\text{ReLU}(\mathbf{a}_c^\top \cdot \mathbf{h}_{v-i}^c))}{\sum_{j=1}^{|\mathbf{rel}^c|} \exp(\text{ReLU}(\mathbf{a}_c^\top \cdot \mathbf{h}_{v-j}^c))}, \quad (5)$$

$$\mathbf{h}_v^c = \sum_{i=1}^{|\mathbf{rel}^c|} \alpha_{v-i}^c \cdot \mathbf{h}_{v-i}^c, \quad (6)$$

where α_{v-i}^c denotes the importance of the i -th type in \mathbf{rel}^c , \mathbf{a}_c represents the trainable attention parameter shared among all common relation types. The encoder for unique relations has the same structure as that for common relations but with different inputs. When learning representations of nodes under each unique relation, we consider integrating the connections of common relations \mathbf{A}^c into another GNN as follows:

$$\mathbf{h}_{v-i}^u = \text{GNN}_u(A_i^u + f_{\text{pool}}^c(\mathbf{A}^c), \mathbf{x}_v), \quad (7)$$

where A_i^u is the i -th relation adjacency matrix in \mathbf{A}^u , and $f_{\text{pool}}^c(\cdot)$ is a pooling function such as *max-pool*(\cdot), *sum-pool*(\cdot), and *mean-pool*(\cdot). We also consider utilizing representations of common relations in the attention mechanism as follows:

$$\alpha_{v-i}^u = \frac{\exp(\text{ReLU}(\mathbf{a}_u^\top \cdot [\mathbf{h}_{v-i}^u || \mathbf{h}_v^c]))}{\sum_{j=1}^{|\mathbf{rel}^u|} \exp(\text{ReLU}(\mathbf{a}_u^\top \cdot [\mathbf{h}_{v-j}^u || \mathbf{h}_v^c]))}, \quad (8)$$

$$\mathbf{h}_v^u = \sum_{i=1}^{|\mathbf{rel}^u|} \alpha_{v-i}^u \cdot \mathbf{h}_{v-i}^u, \quad (9)$$

where α_{v-i}^u denotes the importance of the i -th type in \mathbf{rel}^u , and \mathbf{a}_u represents the trainable attention parameter shared among all unique relation types. Then, to model $q_\phi(\mathbf{e}_2|\mathbf{g}, \mathbf{e}_1)$, we follow Eq. (3) and adopt different MLPs to obtain the distributions related to common relations and unique relations, denoted as $q_\phi(\mathbf{e}_2^c|\mathbf{g}, \mathbf{e}_1)$ and $q_\phi(\mathbf{e}_2^u|\mathbf{g}, \mathbf{e}_1)$, respectively.

Decoder. After adopting the encoder to infer the invariant factors E_2 , our focus shifts to modeling another critical term in $\mathcal{L}_{\text{ELBO}}$, i.e., $p_\theta(\mathbf{y}|\mathbf{g}, \mathbf{e}_1, \mathbf{e}_2)$. We factorize this distribution according to the SCM depicted in Fig. 2 as follows:

$$p_\theta(\mathbf{y}|\mathbf{g}, \mathbf{e}_1, \mathbf{e}_2) = p_\theta(\mathbf{y}|\mathbf{g}, \mathbf{z}_1, \mathbf{z}_2)p_\theta(\mathbf{z}_1|\mathbf{g}, \mathbf{e}_1)p_\theta(\mathbf{z}_2|\mathbf{e}_2). \quad (10)$$

The core focus of the decoder design is to leverage $E_1 = \mathbf{e}_1$ and $E_2 = \mathbf{e}_2$ to capture the latent semantic factors $Z_1 = \mathbf{z}_1$ and $Z_2 = \mathbf{z}_2$. We consider Z_1 and Z_2 to be semantic-level features

derived from information related to the environment and invariant semantic structures, respectively. Accordingly, we first evaluate the connectivity of nodes influenced by \mathbf{e}_1 and \mathbf{e}_2 , generating distinct graph structures that represent different semantics. Then, we implement representation learning within these specific graph structures. In the following steps, we will detail the instantiation of each distribution.

Instantiating $p_\theta(\mathbf{z}_1|\mathbf{g}, \mathbf{e}_1)$ with Multi-layer GNN: We utilize various meta-paths in the subgraph $G_s = \mathbf{g}$ to capture complex semantic information inherent in $E_1 = \mathbf{e}_1$. A meta-path consists of diverse node types and conveys specific semantics, for example, “author-paper-author” indicates author collaboration. Existing works typically require manually defined meta-paths [33]. However, in scenarios involving distribution shifts and few-shot learning, setting and sampling artificial meta-paths is challenging [47]. Therefore, we propose a Multi-layer GNN that automatically captures both short and long meta-paths across various relations. For our input of common relations \mathbf{rel}^c with their adjacency matrices \mathbf{A}^c , and unique relations \mathbf{rel}^u with \mathbf{A}^u , each relation matrix can be considered as a 1-length meta-path graph matrix. We first combine \mathbf{A}^c and \mathbf{A}^u to construct a weighted 1-length meta-path graph matrix:

$$\mathbf{A}_{z_1} = \beta_{z_1} \times f_{pool}^{z_1}(\mathbf{A}^c) + (1 - \beta_{z_1}) \times f_{pool}^{z_1}(\mathbf{A}^u), \quad (11)$$

where β_{z_1} is a trainable smoothing parameter. To extract longer meta-paths, successive multiplications can be performed on the matrix \mathbf{A}_{z_1} . For example, raising \mathbf{A}_{z_1} to the second power automatically incorporates information about 2-length meta-paths. This approach is commonly employed in existing meta-path extraction methods [22], [48]. Therefore, to capture more diverse and longer meta-paths, we extend this approach to a network structure with l layers as follows:

$$\begin{aligned} \mathbf{H}_{z_1}^{(l)} &= \mathbf{A}_{z_1} \cdot \mathbf{H}_{z_1}^{(l-1)} \cdot \mathbf{W}_{z_1}^{(l)} \\ &= \underbrace{\mathbf{A}_{z_1} \cdots \mathbf{A}_{z_1}}_l \cdot \mathbf{X} \cdot \underbrace{\mathbf{W}_{z_1}^{(1)} \cdots \mathbf{W}_{z_1}^{(l)}}_l \\ &= \mathbf{A}_{z_1}^l \cdot \mathbf{X} \cdot \underbrace{\mathbf{W}_{z_1}^{(1)} \cdots \mathbf{W}_{z_1}^{(l)}}_l, \end{aligned} \quad (12)$$

where $\mathbf{H}_{z_1}^{(l)}$ is the hidden embedding of the l -th layer, \mathbf{X} is the node feature matrix of G_s , and $\mathbf{W}_{z_1}^{(l)}$ is the learnable weight matrix that evaluates the influence of meta-paths with l -length on the embedding. Finally, we fuse the outputs of all layers to capture the meta-path information of different lengths across various relations as follows:

$$\begin{aligned} \mathbf{H}_{z_1} &= \frac{1}{l} \sum_{i=1}^l \mathbf{H}_{z_1}^{(i)} \\ &= \frac{1}{l} \sum_{i=1}^l \mathbf{A}_{z_1}^i \cdot \mathbf{H}_{z_1}^{(i-1)} \cdot \mathbf{W}_{z_1}^{(i)}, \end{aligned} \quad (13)$$

where $\mathbf{H}_{z_1}^{(0)}$ is the node feature matrix \mathbf{X} .

Instantiating $p_\theta(\mathbf{z}_2|\mathbf{e}_2)$ with Graph Learner: After utilizing the relation encoder to obtain distributions related to common relations (*i.e.*, $q_\phi(\mathbf{e}_2^c|\mathbf{y}, \mathbf{g}, \mathbf{e}_1)$) and unique relations (*i.e.*,

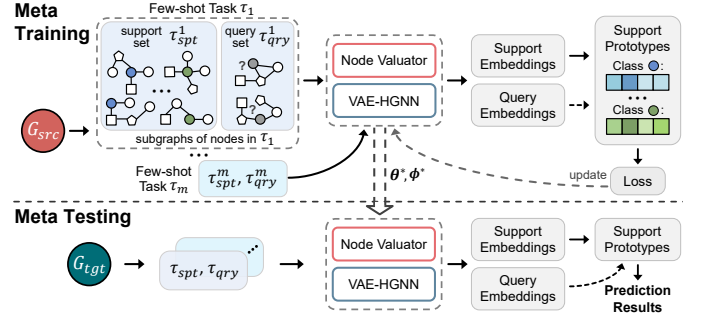


Fig. 4. Meta-learning Framework.

$q_\phi(\mathbf{e}_2^u|\mathbf{y}, \mathbf{g}, \mathbf{e}_1)$), we first sample \mathbf{e}_2^c and \mathbf{e}_2^u from these distributions. Since Z_2 is only determined by E_2 in the SCM, we propose two graph learner modules to learn semantic structures based on \mathbf{e}_2^c and \mathbf{e}_2^u , denoted as $A_{z_2}^c$ and $A_{z_2}^u$, respectively. Both graph learners share the same architecture and we will discuss the graph learner for $A_{z_2}^c$ as an example. Specifically, we introduce a multi-head weighted cosine similarity learning method to compute the connectivity of nodes as follows:

$$a_{uv}^c = \frac{1}{n_{att}} \sum_{i=1}^{n_{att}} \cos(\mathbf{w}_i^c \cdot \mathbf{h}_u^{e_2}, \mathbf{w}_i^c \cdot \mathbf{h}_v^{e_2}), \quad (14)$$

where $\mathbf{h}_u^{e_2}$ and $\mathbf{h}_v^{e_2}$ are node representations in \mathbf{e}_2^c for a node pair (u, v) , the set $\{\mathbf{w}_i^c\}_{i=1}^{n_{att}}$ consists of n_{att} independent learnable weight vectors, which perform similarly as attention mechanisms [49]. After obtaining $A_{z_2}^c$ and $A_{z_2}^u$, we can adopt a trainable parameter β_{z_2} to aggregate them and use a GNN to learn the semantic-level representation of Z_2 as follows:

$$\mathbf{A}_{z_2} = \beta_{z_2} \times \mathbf{A}_{z_2}^c + (1 - \beta_{z_2}) \times \mathbf{A}_{z_2}^u, \quad (15)$$

$$\mathbf{H}_{z_2} = \text{GNN}_{z_2}(\mathbf{A}_{z_2}, \mathbf{X}). \quad (16)$$

Instantiating $p_\theta(\mathbf{y}|\mathbf{g}, \mathbf{z}_1, \mathbf{z}_2)$ with MLP: We can instantiate $p_\theta(\mathbf{y}|\mathbf{g}, \mathbf{z}_1, \mathbf{z}_2)$ using a GNN by inputting G_s with \mathbf{H}_{z_1} and \mathbf{H}_{z_2} . However, considering that \mathbf{H}_{z_1} and \mathbf{H}_{z_2} already contain significant graph structure information from G_s , in order to avoid overfitting, we instantiate $p_\theta(\mathbf{y}|\mathbf{g}, \mathbf{z}_1, \mathbf{z}_2)$ with an MLP as a predictor, *i.e.*, $Y = \text{MLP}(\mathbf{H}_{z_1} + \mathbf{H}_{z_2})$, where $\mathbf{H}_{z_1} + \mathbf{H}_{z_2}$ can be considered as the final embedding output by VAE-HGNN.

C. Meta-Learning

Fig. 4 illustrates an overview of our proposed meta-learning framework, which consists of two steps: meta-training and meta-testing. During meta-training, we utilize the VAE-HGNN module to learn node representations. We also propose a novel *node valuator* module to determine the informativeness of each labeled node. Then, we adopt a prototypical network to transfer generalized knowledge from the source HG to the target HG. During meta-testing, the node valuator is adapted to the target HG to evaluate the importance of few-labeled nodes in OOD environments, thereby facilitating the generation of robust class representations for improved prediction accuracy. **Node Valuator.** In current graph representation learning methods, evaluating the importance of each labeled sample is a

common practice, particularly in cases with a limited sample size [4], [50]. These methods often prioritize nodes with notable centrality and popularity, assuming these nodes to be of greater importance. However, this approach can actually deteriorate the performance of these methods in OOD environments. For instance, a model focusing solely on central nodes might not perform effectively with peripheral nodes.

To overcome this limitation, we adopt a causal perspective to evaluate node importance by examining the richness of node features against distribution shifts. Specifically, we focus on assessing the abundance of node features that remain robust to distribution shifts and determining whether these features are distinctly identifiable. Following the SCM in Fig. 2, our approach includes analyzing the invariant semantic factors Z_2 and distinguishing Z_2 from environmental semantic factors Z_1 . Our approach is guided by the following two key aspects:

1. Structure-level features: The features in both Z_1 and Z_2 are closely related to specific structures with semantics. To improve the distinctiveness of Z_2 , the structural feature differences between Z_1 and Z_2 should be maximized. In addition, Z_2 should exhibit a certain level of connectivity since a lack of connectivity could lead to a structure that lacks meaningful semantics.

2. Node-level features: The node features in Z_1 and Z_2 should also be distinctly different. However, directly comparing the representations of the same node in Z_1 and Z_2 can be influenced by the node's inherent characteristics. Therefore, we propose leveraging the features of neighboring nodes in Z_1 as a reference for more effective comparison.

For the richness of structure-level features, we compare the similarity between $A_{z_1}^{sum}$ and A_{z_2} , and assess the connectivity of A_{z_2} . Here, $A_{z_1}^{sum} = \frac{1}{l} \sum_{i=1}^l A_{z_1}^l$ is derived from the multi-layer GNN module as described in Eq. (13), while A_{z_2} is obtained from the graph learner module as outlined in Eq. (15). The richness score of the structure-level features is defined as:

$$\text{rsl}(v_t) = \cos(A_{z_1}^{sum}, A_{z_2}) + \log\left(\frac{\sum_{i=1}^{|\mathcal{V}_s|} \deg_{z_2}(v_i)}{|\mathcal{V}_s|} + \epsilon\right), \quad (17)$$

where ϵ is a small constant, $\deg_{z_2}(v_i)$ is the in-degree of node v_i in A_{z_2} , and $|\mathcal{V}_s|$ is the number of nodes in the subgraph of v_t (i.e., G_s). For node-level features, we first compute the richness score for each neighbor v_n of v_t :

$$\text{sn}(v_t, v_n) = \tanh(\mathbf{W}_s \cdot [\mathbf{h}_{v_t}^{z_1} \parallel \mathbf{h}_{v_n}^{z_2}]), \quad (18)$$

where $\mathbf{h}_{v_n}^{z_2}$ represents the representation of v_n w.r.t. Z_2 , obtained through Eq. (16), and $\mathbf{h}_{v_t}^{z_1}$ represents the node representation of v_t w.r.t. Z_1 , computed using Eq. (13). \mathbf{W}_s is a learnable weight matrix. Then, we adopt an attention mechanism to compute the importance of the neighbor v_n and compute the node-level richness score as follows:

$$\gamma_{tn} = \frac{\exp(\text{LeakyReLU}(\mathbf{a}_s^\top [\mathbf{h}_{v_t}^{z_2} \parallel \mathbf{h}_{v_n}^{z_2}]))}{\sum_{v_j \in \text{Nei}_t} \exp(\text{LeakyReLU}(\mathbf{a}_s^\top [\mathbf{h}_{v_t}^{z_2} \parallel \mathbf{h}_{v_j}^{z_2}]))}, \quad (19)$$

$$\text{rnl}(v_t) = \sum_{v_i \in \text{Nei}_t} \gamma_{ti} \cdot \text{sn}(v_t, v_i), \quad (20)$$

where Nei_t is the set of neighbors of v_t in A_{z_2} , and \mathbf{a}_s is the trainable attention parameter. Finally, the richness score of a labeled node can be computed as $\text{rs}(v_t) = \text{rsl}(v_t) + \text{rnl}(v_t)$.

Prototypical Network. After obtaining the richness score for each node sample, we follow the idea of the prototypical network [51] and calculate the weighted average of K -shot embedded nodes within class c to derive the class prototype:

$$\text{proto}_c = \sum_{i=1}^K \text{sc}_i \cdot \mathbf{h}_{v_i}, \quad (21)$$

where $\text{sc}_i = \text{rs}(v_i) / \sum_{i=1}^K \text{rs}(v_i)$ is the normalized score, $\mathbf{h}_{v_i} = \mathbf{h}_{v_i}^{z_1} + \mathbf{h}_{v_i}^{z_2}$ is the embedding of node v_i output by VAE-HGNN. The node valuator module is trained through meta-training and is used to compute the class prototype in meta-testing.

Loss Function. During meta-training, the prototype for each class is computed using the nodes in the support set τ^{spl} . To determine the class of a query node u in the query set τ^{qry} , we calculate the probability for each class based on the distance between the node embedding \mathbf{h}_u and each prototype:

$$\text{prob}(c|u) = \frac{\exp(-d(\mathbf{h}_u, \text{proto}_c))}{\sum_{c'} \exp(-d(\mathbf{h}_u, \text{proto}_{c'}))}, \quad (22)$$

where $d(\cdot)$ is a distance metric function and we adopt squared Euclidean distance [51]. Under the episodic training framework, the objective of each meta-training task is to minimize the classification loss between the predictions of the query set and the ground truth. The training loss for a single task τ is the average negative log-likelihood probability of assigning correct class labels as follows:

$$\mathcal{L}_\tau = -\frac{1}{N \times K} \sum_{i=1}^{N \times K} \log(\text{prob}(y_i^* | v_i)), \quad (23)$$

where y_i^* is the ground truth label of v_i . Then, by incorporating the ELBO loss, the total meta-training loss can be defined as:

$$\mathcal{L}_{\text{meta}} = \sum_{j=1}^{|\mathcal{T}_{\text{src}}|} \mathcal{L}_\tau^j + \lambda \mathcal{L}_{\text{ELBO}}^j, \quad (24)$$

where λ is a loss coefficient hyper-parameter for $\mathcal{L}_{\text{ELBO}}$.

VI. EXPERIMENTS AND ANALYSIS

We conduct extensive experiments on seven real-world datasets to answer the following research questions: **RQ1:** How does COHF perform compared with representative and state-of-the-art methods in OOD environments? **RQ2:** How does each of the proposed VAE-HGNN module and node valuator module contribute to the overall performance? **RQ3:** How does COHF perform under different parameter settings?

A. Experimental Settings

Datasets. We adopt seven real-world datasets from three domains: (1) ACM [22] and DBLP [21] from the academic research domain. (2) IMDB [21], MovieLens [52], and Douban [35] from the movie domain. (3) YELP-Restaurant (abbreviated as YELP-R) [32] and YELP-Business (abbreviated as YELP-B) [53] from the business domain. These datasets are publicly available and have been widely used in studies of HGs [35]. Details of these datasets are provided in Table II.

TABLE II
STATISTICS OF DATASETS.

Domain	Dataset	# Nodes	# Relations
Academic	ACM	# authors (A): 5,912 # papers (P): 3,025 # subjects (S): 57	# A-P: 9,936 # P-S: 3,025
	DBLP	# authors (A): 4,057 # papers (P): 14,328 # terms (T): 7,723 # venues (V): 20	# A-P: 19,645 # P-T: 85,810 # P-V: 14,328
Movie	IMDB	# movies (M): 4,278 # directors (D): 2,081 # actors (A): 5,257	# M-D: 4,278 # M-A: 12,828
	MovieLens	# movies (M): 1,682 # users (U): 943 # occupations (O): 21 # ages (E): 8	# U-M: 100,000 # U-E: 943 # U-O: 943
	Douban	# movies (M): 12,677 # directors (D): 2,449 # actors (A): 6,311 # users (U): 13,367 # groups (G): 2,753	# M-D: 11,276 # M-A: 33,587 # U-M: 355,072 # U-G: 127,632 # U-U: 392,519
Business	YELP-R	# businesses (B): 2,614 # users (U): 1,286 # services (S): 2 # star levels (L): 9 # reservations (R): 2	# B-U: 30,838 # B-R: 2,614 # B-S: 2,614 # B-L: 2,614
	YELP-B	# businesses (B): 7,474 # phrases (P): 74,943 # star levels (L): 9 # locations (O): 39	# B-P: 27,209,836 # B-L: 7,474 # B-O: 7,474 # P-P: 2,654,313

Meta-learning and OOD Settings. We consider the following two distinct scenarios:

1. Inter-dataset setting: This setting involves utilizing two different datasets from the same domain. One dataset is randomly chosen as the source HG, and another from the same domain is selected as the target HG. Note that there are inherent differences between datasets within the same domain, such as varying node and relationship types, different node features, and diverse graph structures. These differences lead to multiple distribution shifts between the source HG and the target HG. Furthermore, to simulate distribution shifts between training and testing data in the target HG, we follow the approach in [54], which generates training and testing data with distribution shifts based on node degrees.

2. Intra-dataset setting: In this setting, both the source HG and target HG come from the same dataset. We create I.I.D. and OOD data to evaluate the method’s effectiveness against distribution shifts. Note that in few-shot learning, the labeled nodes in source HG and target HG must have different classes. For instance, in the source HG, only *action* and *musical* “movie” nodes are labeled, while in the target HG, *family* and *romantic* “movie” nodes are labeled. This requires datasets with a wide variety of node classes. To this end, we use three datasets: Douban (38 “movie” node classes), MovieLens (18 “movie” node classes), and YELP-B (16 “business” node classes). The classes in each dataset are evenly split into two groups: one for the source HG, where nodes from these classes are labeled, and the other for the target HG.

To create I.I.D. data within a single dataset, we randomly divide the dataset into three splits with similar sizes, which are designated as the source HG, training data, and testing data. For OOD data, we firstly follow [54] to generate three splits with distribution shifts based on node degrees. Then,

TABLE III
NODE CLASSIFICATION ACCURACY IN INTRA-DATASET SETTING.

	Douban			MovieLens			YELP-B		
	I.I.D.	OOD	Drop	I.I.D.	OOD	Drop	I.I.D.	OOD	Drop
2-way 1-shot									
GAT	0.5107	0.4560	12.00%	0.5477	0.5137	6.62%	0.5107	0.4933	3.53%
SGC	0.5093	0.4983	2.21%	0.5563	0.5183	7.33%	0.5280	0.5152	2.48%
GIN	0.5153	0.4813	7.06%	0.5743	0.5387	6.61%	0.5283	0.5094	3.71%
HAN	0.5473	0.5233*	4.59%	0.5833	0.5567	4.78%	0.5517	0.5217	5.75%
MAGNN	0.5522	0.5156	7.10%	0.6022	0.5633	6.91%	0.5544	0.5133	8.01%
CAL	0.5018	0.4947	1.44%	0.5173	0.5019	3.07%	0.5127	0.5110	0.33%
DIR	0.5142	0.4996	2.92%	0.5228	0.4893	6.85%	0.5117	0.5107	0.20%
WSGNN	0.5042	0.4872	3.49%	0.5156	0.4978	3.58%	0.5211	0.5178	0.64%
MAML	0.5063	0.5053	0.20%	0.5317	0.5157	3.10%	0.5223	0.5033	3.78%
ProtoNet	0.5087	0.4893	3.96%	0.5427	0.5200	4.37%	0.5173	0.5003	3.40%
Meta-GNN	0.5114	0.4773	7.14%	0.5473	0.5192	5.41%	0.5260	0.4964	5.96%
GPN	0.5037	0.4717	6.78%	0.5550	0.5173	7.29%	0.5377	0.5037	6.75%
G-Meta	0.5556	0.4889	13.64%	0.5677	0.5326	6.59%	0.5859*	0.5222	12.20%
CGFL	0.5612*	0.5077	10.54%	0.6289*	0.6011*	4.62%	0.5783	0.5433*	6.44%
HG-Meta	0.5183	0.4817	7.60%	0.5933	0.5573	6.46%	0.5413	0.5207	3.96%
COHF	0.5863 ¹	0.5652	3.73%	0.6537	0.6356	2.85%	0.5903	0.5811	1.58%
Improvement ²	4.47%	8.01%		3.94%	5.74%		0.75%	6.96%	
3-way 3-shot									
GAT	0.3436	0.2669	28.74%	0.4778	0.4018	18.91%	0.3556	0.3369	5.55%
SGC	0.3447	0.2987	15.40%	0.4716	0.3656	28.99%	0.3633	0.3309	9.79%
GIN	0.3423	0.3049	12.27%	0.4916	0.4164	18.06%	0.3609	0.3327	8.48%
HAN	0.3612	0.3011	19.96%	0.4922	0.4456	10.46%	0.3744	0.3467	7.99%
MAGNN	0.3581	0.3163	13.22%	0.5311	0.4719*	12.55%	0.3756	0.3474	8.12%
CAL	0.3413	0.3361	1.55%	0.3598	0.3442	4.53%	0.3469	0.3367	3.03%
DIR	0.3467	0.3335	3.96%	0.4044	0.3362	20.29%	0.3520	0.3404	3.41%
WSGNN	0.3433	0.3404	0.85%	0.3615	0.3319	8.92%	0.3444	0.3356	2.62%
MAML	0.3424	0.3309	3.48%	0.3464	0.3338	3.77%	0.3418	0.3364	1.61%
ProtoNet	0.3351	0.3333	0.54%	0.4564	0.3484	31.00%	0.3384	0.3331	1.59%
Meta-GNN	0.3465	0.3274	5.83%	0.4961	0.4123	20.33%	0.3692	0.3407	8.37%
GPN	0.3476	0.3333	4.29%	0.4413	0.3873	13.94%	0.3722	0.3322	12.04%
G-Meta	0.3667	0.3432	6.85%	0.5189	0.4211	23.22%	0.3764	0.3603	4.47%
CGFL	0.3711*	0.3509*	5.76%	0.5259	0.4478	17.44%	0.3798*	0.3625*	4.77%
HG-Meta	0.3652	0.3412	7.03%	0.5313*	0.4609	15.27%	0.3713	0.3551	4.56%
COHF	0.3829	0.3754	2.00%	0.5423	0.5137	5.57%	0.3957	0.3892	1.67%
Improvement ²	3.18%	6.98%		2.07%	8.86%		4.19%	7.37%	

* Result of the best-performing baseline.

¹ Results of the best-performing method are in bold.

² Improvements of COHF over the best-performing baseline are underlined.

we introduce heterogeneity-level shifts by either reducing node types (excluding the target node type) or keeping them unchanged in each split. These splits are randomly assigned as the source HG, training data, and testing data. We repeat the above two construction processes five times for each dataset, creating five I.I.D. and five OOD datasets. Finally, for one dataset under I.I.D. or OOD settings, we average the experimental results from its five corresponding generated datasets to derive the final results.

Baselines. Given the lack of specialized solutions for OOD generalization in HGFL problems, we select 16 representative and state-of-the-art methods as baselines, which can be adapted to our meta-learning and OOD settings with minor modifications. These baselines can be categorized into six groups: (1) **Homogeneous GNNs:** *GAT* [55], *SGC* [56] and *GIN* [57]. (2) **Heterogeneous GNNs:** *HAN* [20] and *MAGNN* [21]. (3) **Graph OOD generalization methods:** *CAL* [30], *DIR* [13], and *WSGNN* [58]. (4) **Few-shot learning methods:** *MAML* [15] and *ProtoNet* [51]. (5) **Homogeneous graph few-shot learning methods:** *Meta-GNN* [23], *GPN* [50] and *G-Meta* [16]. (6) **Heterogeneous graph few-shot learning methods:** *CGFL* [4] and *HG-Meta* [7].

Parameter Settings. In the N -way K -shot setting, N is set to $\{2, 3\}$ and K is set to $\{1, 3, 5\}$. The number of tasks m is set to

TABLE IV
NODE CLASSIFICATION ACCURACY IN INTER-DATASET SETTING.

	ACM-DBLP		DBLP-ACM		IMDB-Douban		Douban-IMDB		MvLens-Douban		Douban-MvLens		YELP R-B		YELP B-R	
	2-way	3-way	2-way	3-way	2-way	3-way	2-way	3-way	2-way	3-way	2-way	3-way	2-way	3-way	2-way	3-way
<i>1-shot</i>																
GAT	0.7133	0.5489	0.6297	0.4733	0.4017	0.3052	0.5167	0.3458	0.4590	0.2907	0.5050	0.3458	0.5043	0.3413	0.5470	0.3544
SGC	0.7147	0.6057	0.5698	0.4652	0.4932	0.3235	0.5147	0.3512	0.4953	0.3269	0.5174	0.3414	0.5077	0.3469	0.5118	0.3625
GIN	0.6984	0.5106	0.5982	0.4522	0.4453	0.2909	0.5222	0.3615	0.4431	0.2591	0.5117	0.3475	0.5126	0.3370	0.5930	0.4368
HAN	0.8088	0.6417	0.7453*	0.6071	0.4937	0.3240	0.5240	0.3622	0.4313	0.2767	0.5340	0.3531	0.5283	0.3651	0.6417	0.4633
MAGNN	0.8112	0.6713	0.7359	0.6172*	0.4967	0.3252	0.5355	0.3659	0.5150	0.3469*	0.5411	0.3804	0.5278	0.3607	0.6244	0.4674
CAL	0.5023	0.3288	0.5490	0.3296	0.4898	0.3219	0.5094	0.3370	0.4950	0.3367	0.4913	0.3352	0.5063	0.3339	0.5060	0.3412
DIR	0.5939	0.4880	0.6359	0.4943	0.4313	0.2710	0.5117	0.3477	0.4283	0.2632	0.4871	0.3229	0.5027	0.3345	0.5722	0.4284
WSGNN	0.5300	0.3489	0.5037	0.3347	0.5003	0.3321	0.4828	0.3240	0.5017	0.3345	0.4767	0.3408	0.5117	0.3186	0.4834	0.3267
MAML	0.6339	0.4551	0.5740	0.3896	0.4991	0.3285	0.4971	0.3345	0.4975	0.3332	0.5008	0.3384	0.4976	0.3317	0.5109	0.3436
ProtoNet	0.5580	0.3949	0.5636	0.3939	0.4838	0.3119	0.5068	0.3436	0.4758	0.2986	0.5157	0.3473	0.4990	0.3338	0.5026	0.3439
Meta-GNN	0.7099	0.5915	0.6509	0.5312	0.4844	0.3261	0.5167	0.3448	0.4924	0.3342	0.5227	0.3523	0.5002	0.3324	0.5316	0.3536
GPN	0.6122	0.4518	0.7099	0.5355	0.4501	0.2920	0.5032	0.3389	0.5004	0.3337	0.4928	0.3335	0.5001	0.3334	0.5127	0.4016
G-Meta	0.6879	0.5377	0.5744	0.4007	0.4907	0.3404*	0.5370	0.3273	0.4795	0.3301	0.5194	0.3929*	0.5145	0.3665	0.5291	0.3768
CGFL	0.8240*	0.7211*	0.7413	0.6049	0.5150*	0.3080	0.5374*	0.3714*	0.5290*	0.3153	0.5467	0.3701	0.5358*	0.3769*	0.6509*	0.4797*
HG-Meta	0.7940	0.7031	0.7337	0.5631	0.5038	0.3176	0.5320	0.3653	0.4610	0.2944	0.5514*	0.3840	0.5216	0.3489	0.6316	0.4609
COHF	0.8463¹	0.7413	0.7711	0.6354	0.5269	0.3543	0.5650	0.3962	0.5662	0.3706	0.5844	0.3968	0.5644	0.4019	0.6675	0.4913
Improvement ²	<u>2.71%</u>	<u>2.80%</u>	<u>3.46%</u>	<u>2.95%</u>	<u>2.31%</u>	<u>4.08%</u>	<u>5.14%</u>	<u>6.68%</u>	<u>7.03%</u>	<u>6.83%</u>	<u>5.98%</u>	<u>0.99%</u>	<u>5.34%</u>	<u>6.63%</u>	<u>2.55%</u>	<u>2.42%</u>
<i>3-shot</i>																
GAT	0.8162	0.6733	0.6760	0.5549	0.4067	0.3122	0.5429	0.3880	0.4416	0.2622	0.5355	0.4014	0.5189	0.3469	0.5509	0.4087
SGC	0.8107	0.6788	0.6944	0.5577	0.4878	0.3104	0.5461	0.3707	0.4790	0.3235	0.5065	0.4050	0.5031	0.3478	0.5416	0.4378
GIN	0.7694	0.6204	0.6787	0.5542	0.3909	0.2975	0.5457	0.3858	0.4764	0.2428	0.5429	0.4376	0.5093	0.3619	0.6662	0.5118
HAN	0.8795	0.7532	0.8233	0.6052	0.4923	0.3091	0.5583	0.3962*	0.3770	0.2824	0.5631	0.3932	0.5267	0.3667	0.6811	0.5378
MAGNN	0.8912	0.7641	0.8325*	0.5227	0.5075*	0.3445	0.5461	0.3937	0.5204	0.3441	0.5849	0.4522*	0.5255	0.3533	0.6930	0.4636
CAL	0.5193	0.3382	0.4974	0.3303	0.4917	0.3229	0.5183	0.3352	0.5053	0.3393	0.5307	0.3370	0.5106	0.3313	0.5130	0.3457
DIR	0.6897	0.5600	0.6760	0.5371	0.4333	0.2880	0.5339	0.3658	0.4343	0.2932	0.5060	0.3400	0.5157	0.3547	0.6323	0.4704
WSGNN	0.4518	0.3378	0.5183	0.3412	0.5011	0.3444	0.5122	0.3341	0.3586	0.3370	0.5011	0.3526	0.4822	0.3489	0.4878	0.3378
MAML	0.7288	0.5409	0.6248	0.4968	0.4962	0.3345	0.5084	0.3347	0.5014	0.3369	0.4986	0.3409	0.5098	0.3413	0.5052	0.3572
ProtoNet	0.5634	0.4175	0.5438	0.4285	0.4992	0.3325	0.5036	0.3397	0.4988	0.3307	0.5174	0.3495	0.5066	0.3392	0.5062	0.3544
Meta-GNN	0.8328	0.6939	0.7429	0.6126	0.4953	0.3341	0.5443	0.3708	0.4998	0.3435	0.5502	0.3759	0.4995	0.3334	0.5498	0.3625
GPN	0.7631	0.5636	0.6726	0.4903	0.4542	0.3015	0.5154	0.3461	0.4915	0.3415	0.4703	0.3071	0.512	0.3576	0.5710	0.4569
G-Meta	0.7324	0.5114	0.6958	0.6027	0.4965	0.3569*	0.4919	0.3411	0.5056	0.3433	0.6056*	0.3778	0.5247	0.3912*	0.6833	0.3222
CGFL	0.9241*	0.8178*	0.8207	0.6368	0.4956	0.3444	0.5643*	0.3896	0.5398*	0.3571	0.5823	0.4116	0.5404*	0.3815	0.6947*	0.5429*
HG-Meta	0.9062	0.8136	0.7882	0.6491*	0.4672	0.2985	0.5564	0.3911	0.4766	0.3628*	0.5988	0.4424	0.5254	0.3575	0.5858	0.4224
COHF	0.9353	0.8335	0.8631	0.6933	0.5462	0.3812	0.5931	0.4229	0.5750	0.3867	0.6151	0.4602	0.5769	0.4175	0.7171	0.5653
Improvement ²	<u>1.21%</u>	<u>1.92%</u>	<u>3.68%</u>	<u>6.81%</u>	<u>7.63%</u>	<u>6.81%</u>	<u>5.10%</u>	<u>6.74%</u>	<u>6.52%</u>	<u>6.59%</u>	<u>1.57%</u>	<u>1.77%</u>	<u>6.75%</u>	<u>6.72%</u>	<u>3.22%</u>	<u>4.13%</u>

* Result of the best-performing baseline. ¹ Results of the best-performing method are in bold. ² Improvements of COHF over the best-performing baseline are underlined.

100 for all datasets. To ensure fair comparisons, the embedding dimension is set to 64 for both the baselines and COHF. The baseline parameters are initially set to the values reported in the original papers and are further optimized through grid-searching to achieve optimal performance. For COHF, the subgraph G_s is constructed by sampling 2-hop neighbors of the target node. The dimension of \mathbf{e}_2 (D) is set to 64. In the relation encoder module, we adopt two GCNs [59] as GNN_c and GNN_u , $f_{pool}^c(\cdot)$ is set to *max-pooling*(\cdot). In the multi-layer GNN module, $f_{pool}^{z_1}(\cdot)$ uses *max-pooling*(\cdot), and the number of GNN layers (l) is set to 2. In the graph learner module, we continue to use GCN as GNN_{z_2} , and n_{att} is set to 8. In the meta-learning module, the loss coefficient λ is set to 0.4.

Evaluation Metrics. We adopt two widely used node classification metrics: *Accuracy* and *Macro-F1 score* [23], [55]. To ensure a fair and accurate assessment of the performance of all methods, we perform 10 independent runs for each N -way K -shot setting and report the average results.

B. Experimental Results

Performance Comparison with Baselines (RQ1). Tables III-V present the performance comparison between COHF

and baselines in both intra-dataset and inter-dataset settings. The results demonstrate a significant improvement of COHF over the best-performing baselines. Across all settings, COHF consistently outperforms the baselines in terms of accuracy and F1-score. Due to space constraints, Table V only includes a subset of the F1-score results. Specifically, in the intra-dataset setting, COHF achieves an average increase of 7.32% in accuracy and 8.07% in F1-score. In the inter-dataset setting, COHF achieves an average improvement of 4.53% in accuracy and 4.71% in F1-score. These improvements are primarily attributed to our proposed VAE-HGNN module and the node valuator module. The VAE-HGNN module, innovatively designed based on our SCM model, effectively extracts invariant factors in OOD environments. Meanwhile, the node valuator module enhances knowledge transfer across HGs with distribution shifts and few-labeled data. In contrast, the baseline methods either overlook OOD environments in few-shot learning or focus solely on OOD problems within homogeneous graphs. Such limitations hinder their ability to extract generalized semantic knowledge from the source HG, leading to inferior performance when applied to a target HG

TABLE V
NODE CLASSIFICATION F1-SCORE IN 2-WAY 3-SHOT SETTING.

	GAT	SGC	GIN	HAN	MAGNN	CAL	DIR	WSGNN	MAML	ProtoNet	Meta-GNN	GNP	G-Meta	CGFL	HG-Meta	COHF	Improv. ²
ACM-DBLP	0.8114	0.7973	0.7639	0.8648	0.8896	0.5193	0.6419	0.4540	0.6822	0.4736	0.8241	0.7520	0.6926	0.9136*	0.9041	0.9394 ¹	<u>2.82%</u>
Douban-MvLens	0.5046	0.5056	0.5188	0.5486	0.5588	0.5285	0.4269	0.4710	0.4714	0.4452	0.5389	0.4208	0.6004*	0.5802	0.5807	0.6279	<u>4.58%</u>
YELP B-R	0.5269	0.5478	0.6172	0.6809	0.6879	0.4883	0.6127	0.4856	0.4887	0.4476	0.5456	0.5485	0.6812	0.6973*	0.5692	0.7239	<u>3.81%</u>
MvLens (I.I.D.)	0.5939	0.6012	0.6083	0.6501*	0.6345	0.5110	0.5362	0.5132	0.5090	0.4324	0.6105	0.5949	0.6447	0.6479	0.6426	0.6815	<u>4.83%</u>
MvLens (OOD)	0.5468	0.5134	0.5467	0.5813	0.5881	0.4973	0.4495	0.4697	0.4899	0.4138	0.5559	0.5353	0.6055	0.6183*	0.5887	0.6691	<u>8.22%</u>
Drop	8.61%	17.10%	11.27%	11.84%	7.89%	2.75%	19.29%	9.26%	3.90%	4.49%	9.82%	11.13%	6.47%	4.79%	9.16%	1.85%	

* Result of the best-performing baseline. ¹ Results of the best-performing method are in bold. ² Improvements of COHF over the best-performing baseline are underlined.

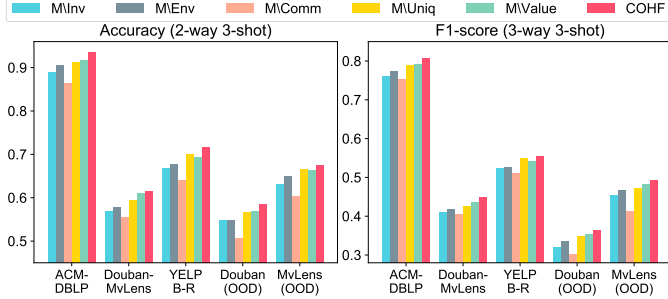


Fig. 5. Node classification performance of COHF variants.

with different distributions and limited labeled data.

Furthermore, it is worth noting that in Tables III and V, almost all baseline methods demonstrate a significant drop in performance when transitioning from I.I.D. to OOD settings. This decline is especially evident in methods such as CGFL, G-Meta, and MAGNN, which perform well in I.I.D. settings. On average, there is a notable decrease of 7.84% in accuracy and 9.19% in F1-score across all baselines. In contrast, COHF exhibits a relatively minor average decrease of 2.9% in accuracy and 1.85% in F1-score. This underlines the robustness of our approach in handling distribution shifts in HGFL.

Ablation Study (RQ2). To investigate the impact of the core modules of COHF, we create five variants focusing on three key aspects: (1) Two variants are created to explore the impact of the environmental and invariant information captured by VAE-HGNN. The **M\Inv** variant focuses on environmental information by removing the relation encoder and graph learner modules. In contrast, the **M\Env** variant emphasizes invariant information by excluding the multi-layer GNN module. (2) Two variants are created to evaluate the effectiveness of leveraging common and unique relations for OOD generalization. The **M\Comm** variant focuses on unique relations by setting the common relation adjacency matrices A^c as unit diagonal matrices. Conversely, the **M\Uniq** variant emphasizes common relations by setting A^u as unit diagonal matrices. (3) The **M\Value** variant is created to investigate the effectiveness of the node valuator module by removing it. From Fig. 5, we have the following observations:

- The **M\Inv** and **M\Env** variants exhibit inferior performance compared to the original COHF. This highlights the important role of both environmental and invariant features in determining node labels.
- The **M\Comm** and **M\Uniq** variants are outperformed by

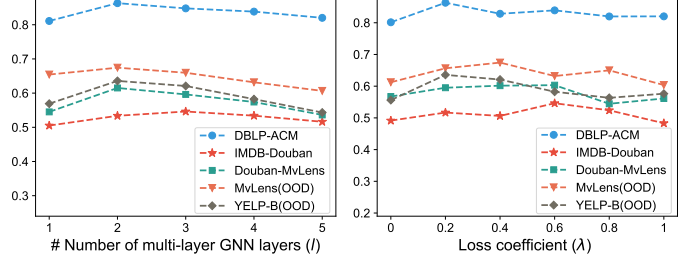


Fig. 6. 2-way 3-shot node classification accuracy of COHF with different parameter settings.

COHF, indicating that adopting a relation-level perspective and utilizing common and unique relations is beneficial for identifying features that are resilient to distribution shifts.

- The **M\Value** variant demonstrates lower performance than COHF, emphasizing the significance of the valuator module. This module not only assesses the richness of environment-independent features of nodes in the source HG, but also evaluates the significance of few-labeled nodes in deriving robust prototypes for the target HG.

Parameter Study (RQ3). We investigate the sensitivity of several important parameters in COHF and illustrate their impacts in Fig. 6. For the number of layers in the multi-layer GNN module, moderate values of 2 or 3 are recommended. This is mainly because meta-paths of lengths 2 and 3 are usually sufficient to capture the necessary semantic information for node classification. Meta-paths longer than these do not typically lead to further performance improvements. For the loss coefficient λ , COHF achieves optimal performance when λ ranges between 0.2 to 0.6. Values of λ that are either too small or too large can lead to degraded performance.

VII. CONCLUSION

In this paper, we introduce a novel problem of OOD generalization in heterogeneous graph few-shot learning, and propose a solution called COHF. Following the invariance principle from causal theory, COHF leverages invariant factors to address distribution shifts across HGs. Furthermore, COHF integrates a novel value-based meta-learning framework, which facilitates learning new classes with few-labeled data and varying distributions. Extensive experiments demonstrate the superior performance of COHF. For future work, we plan to explore the application of COHF in other graph learning tasks, such as link prediction and relation mining, to exploit its potential across a wider range of contexts.

REFERENCES

- [1] C. Shi, Y. Li, J. Zhang, Y. Sun, and S. Y. Philip, “A survey of heterogeneous information network analysis,” *IEEE TKDE*, vol. 29, no. 1, pp. 17–37, 2016.
- [2] C. Zhang, K. Ding, J. Li, X. Zhang, Y. Ye, N. V. Chawla, and H. Liu, “Few-shot learning on graphs: A survey,” *arXiv preprint arXiv:2203.09308*, 2022.
- [3] M. Yoon, J. Palowitch, D. Zelle, Z. Hu, R. Salakhutdinov, and B. Perozzi, “Zero-shot transfer learning within a heterogeneous graph via knowledge transfer networks,” in *NIPS*, 2022, pp. 27 347–27 359.
- [4] P. Ding, Y. Wang, and G. Liu, “Cross-heterogeneity graph few-shot learning,” in *CIKM*, 2023, pp. 420–429.
- [5] Z. Zhuang, X. Xiang, S. Huang, and D. Wang, “Hinfshot: A challenge dataset for few-shot node classification in heterogeneous information network,” in *ICMR*, 2021, pp. 429–436.
- [6] P. Ding, Y. Wang, G. Liu, and X. Zhou, “Few-shot semantic relation prediction across heterogeneous graphs,” *IEEE TKDE*, vol. 35, no. 10, pp. 10 265–10 280, 2023.
- [7] Q. Zhang, X. Wu, Q. Yang, C. Zhang, and X. Zhang, “Hg-meta: Graph meta-learning over heterogeneous graphs,” in *SDM*, 2022, pp. 397–405.
- [8] Y. Bengio, T. Deleu, N. Rahaman, R. Ke, S. Lachapelle, O. Bilaniuk, A. Goyal, and C. Pal, “A meta-transfer objective for learning to disentangle causal mechanisms,” *arXiv preprint arXiv:1901.10912*, 2019.
- [9] J. Pearl, *Causality*. Cambridge university press, 2009.
- [10] M. Rojas-Carulla, B. Schölkopf, R. Turner, and J. Peters, “Invariant models for causal transfer learning,” *JMLR*, vol. 19, no. 1, pp. 1309–1342, 2018.
- [11] Y. Lin, H. Dong, H. Wang, and T. Zhang, “Bayesian invariant risk minimization,” in *CVPR*, 2022, pp. 16 021–16 030.
- [12] Y. Chen, Y. Zhang, Y. Bian, H. Yang, M. Kaili, B. Xie, T. Liu, B. Han, and J. Cheng, “Learning causally invariant representations for out-of-distribution generalization on graphs,” *NIPS*, vol. 35, pp. 22 131–22 148, 2022.
- [13] S. Fan, X. Wang, Y. Mo, C. Shi, and J. Tang, “Debiasing graph neural networks via learning disentangled causal substructure,” *NIPS*, vol. 35, pp. 24 934–24 946, 2022.
- [14] W. Wang, X. Lin, F. Feng, X. He, M. Lin, and T.-S. Chua, “Causal representation learning for out-of-distribution recommendation,” in *WWW*, 2022, pp. 3562–3571.
- [15] C. Finn, P. Abbeel, and S. Levine, “Model-agnostic meta-learning for fast adaptation of deep networks,” in *ICML*, 2017, pp. 1126–1135.
- [16] K. Huang and M. Zitnik, “Graph meta learning via local subgraphs,” *NIPS*, vol. 33, pp. 5862–5874, 2020.
- [17] H. Hong, H. Guo, Y. Lin, X. Yang, Z. Li, and J. Ye, “An attention-based graph neural network for heterogeneous structural learning,” in *AAAI*, vol. 34, no. 04, 2020, pp. 4132–4139.
- [18] Q. Lv, M. Ding, Q. Liu, Y. Chen, W. Feng, S. He, C. Zhou, J. Jiang, Y. Dong, and J. Tang, “Are we really making much progress? revisiting, benchmarking and refining heterogeneous graph neural networks,” in *KDD*, 2021, pp. 1150–1160.
- [19] Z. Zhou, J. Shi, R. Yang, Y. Zou, and Q. Li, “Slotgat: slot-based message passing for heterogeneous graphs,” in *ICML*, 2023, pp. 42 644–42 657.
- [20] X. Wang, H. Ji, C. Shi, B. Wang, Y. Ye, P. Cui, and P. S. Yu, “Heterogeneous graph attention network,” in *WWW*, 2019, pp. 2022–2032.
- [21] X. Fu, J. Zhang, Z. Meng, and I. King, “Magann: Metapath aggregated graph neural network for heterogeneous graph embedding,” in *WWW*, 2020, pp. 2331–2341.
- [22] S. Yun, M. Jeong, R. Kim, J. Kang, and H. J. Kim, “Graph transformer networks,” *NIPS*, vol. 32, 2019.
- [23] F. Zhou, C. Cao, K. Zhang, G. Trajcevski, T. Zhong, and J. Geng, “Meta-gnn: On few-shot node classification in graph meta-learning,” in *CIKM*, 2019, pp. 2357–2360.
- [24] Q. Zhang, X. Wu, Q. Yang, C. Zhang, and X. Zhang, “Few-shot heterogeneous graph learning via cross-domain knowledge transfer,” in *KDD*, 2022, pp. 2450–2460.
- [25] A. Baranwal, K. Fountoulakis, and A. Jagannath, “Graph convolution for semi-supervised classification: Improved linear separability and out-of-distribution generalization,” *arXiv preprint arXiv:2102.06966*, 2021.
- [26] B. Bevilacqua, Y. Zhou, and B. Ribeiro, “Size-invariant graph representations for graph classification extrapolations,” in *ICML*, 2021, pp. 837–851.
- [27] C.-Y. Chuang and S. Jegelka, “Tree mover’s distance: Bridging graph metrics and stability of graph neural networks,” *NIPS*, vol. 35, pp. 2944–2957, 2022.
- [28] D. Krueger, E. Caballero, J.-H. Jacobsen, A. Zhang, J. Binas, D. Zhang, R. Le Priol, and A. Courville, “Out-of-distribution generalization via risk extrapolation (rex),” in *ICML*, 2021, pp. 5815–5826.
- [29] Y.-X. Wu, X. Wang, A. Zhang, X. He, and T.-S. Chua, “Discovering invariant rationales for graph neural networks,” *arXiv preprint arXiv:2201.12872*, 2022.
- [30] Y. Sui, X. Wang, J. Wu, M. Lin, X. He, and T.-S. Chua, “Causal attention for interpretable and generalizable graph classification,” in *KDD*, 2022, pp. 1696–1705.
- [31] Y. Lu, C. Shi, L. Hu, and Z. Liu, “Relation structure-aware heterogeneous information network embedding,” in *AAAI*, 2019, pp. 4456–4463.
- [32] C. Shi, Y. Lu, L. Hu, Z. Liu, and H. Ma, “Rhine: relation structure-aware heterogeneous information network embedding,” *IEEE TKDE*, vol. 34, no. 1, pp. 433–447, 2020.
- [33] Y. Yang, J. Han, X. Yan, P. S. Yu, and T. Wu, “Pathsim: Meta path-based top-k similarity search in heterogeneous information networks,” *PVLDB*, vol. 4, no. 11, pp. 992–1003, 2011.
- [34] Y. Fang, W. Lin, V. W. Zheng, M. Wu, J. Shi, K. C.-C. Chang, and X.-L. Li, “Metagraph-based learning on heterogeneous graphs,” *IEEE TKDE*, vol. 33, no. 1, pp. 154–168, 2019.
- [35] X. Wang, D. Bo, C. Shi, S. Fan, Y. Ye, and S. Y. Philip, “A survey on heterogeneous graph embedding: methods, techniques, applications and sources,” *IEEE Transactions on Big Data*, vol. 9, no. 2, pp. 415–436, 2022.
- [36] X. Li, D. Ding, B. Kao, Y. Sun, and N. Mamoulis, “Leveraging meta-path contexts for classification in heterogeneous information networks,” in *ICDE*, 2021, pp. 912–923.
- [37] Y. Yang, Z. Guan, J. Li, W. Zhao, J. Cui, and Q. Wang, “Interpretable and efficient heterogeneous graph convolutional network,” *IEEE TKDE*, 2021.
- [38] M. Zhang and Y. Chen, “Link prediction based on graph neural networks,” *NIPS*, vol. 31, 2018.
- [39] H. Zeng, H. Zhou, A. Srivastava, R. Kannan, and V. Prasanna, “Graphsaint: Graph sampling based inductive learning method,” *arXiv preprint arXiv:1907.04931*, 2019.
- [40] C. Donnat, M. Zitnik, D. Hallac, and J. Leskovec, “Learning structural node embeddings via diffusion wavelets,” in *KDD*, 2018, pp. 1320–1329.
- [41] J. Pearl and D. Mackenzie, *The book of why: the new science of cause and effect*. Basic books, 2018.
- [42] D. P. Kingma, S. Mohamed, D. Jimenez Rezende, and M. Welling, “Semi-supervised learning with deep generative models,” *NIPS*, vol. 27, 2014.
- [43] D. P. Kingma and M. Welling, “Auto-encoding variational bayes,” *arXiv preprint arXiv:1312.6114*, 2013.
- [44] M. Simonovsky and N. Komodakis, “Graphvae: Towards generation of small graphs using variational autoencoders,” in *ICANN*, 2018, pp. 412–422.
- [45] H. Wang, C. Zhou, X. Chen, J. Wu, S. Pan, and J. Wang, “Graph stochastic neural networks for semi-supervised learning,” *NIPS*, vol. 33, pp. 19 839–19 848, 2020.
- [46] J. Ma, W. Tang, J. Zhu, and Q. Mei, “A flexible generative framework for graph-based semi-supervised learning,” *NIPS*, vol. 32, 2019.
- [47] T. Chen and Y. Sun, “Task-guided and path-augmented heterogeneous network embedding for author identification,” in *WSDM*, 2017, pp. 295–304.
- [48] J. Gasteiger, A. Bojchevski, and S. Günnemann, “Predict then propagate: Graph neural networks meet personalized pagerank,” *arXiv preprint arXiv:1810.05997*, 2018.
- [49] A. Vaswani, N. Shazeer, N. Parmar, J. Uszkoreit, L. Jones, A. N. Gomez, Ł. Kaiser, and I. Polosukhin, “Attention is all you need,” *NIPS*, vol. 30, 2017.
- [50] K. Ding, J. Wang, J. Li, K. Shu, C. Liu, and H. Liu, “Graph prototypical networks for few-shot learning on attributed networks,” in *CIKM*, 2020, pp. 295–304.
- [51] J. Snell, K. Swersky, and R. Zemel, “Prototypical networks for few-shot learning,” in *NIPS*, 2017, pp. 4077–4087.
- [52] B. N. Miller, I. Albert, S. K. Lam, J. A. Konstan, and J. Riedl, “Movielens unplugged: experiences with an occasionally connected recommender system,” in *IUI*, 2003, pp. 263–266.

- [53] C. Yang, Y. Xiao, Y. Zhang, Y. Sun, and J. Han, "Heterogeneous network representation learning: A unified framework with survey and benchmark," *IEEE TKDE*, vol. 34, no. 10, pp. 4854–4873, 2020.
- [54] S. Gui, X. Li, L. Wang, and S. Ji, "Good: A graph out-of-distribution benchmark," *NIPS*, vol. 35, pp. 2059–2073, 2022.
- [55] P. Velickovic, G. Cucurull, A. Casanova, A. Romero, P. Lio, Y. Bengio *et al.*, "Graph attention networks," *stat*, vol. 1050, no. 20, pp. 10–48 550, 2017.
- [56] F. Wu, A. Souza, T. Zhang, C. Fifty, T. Yu, and K. Weinberger, "Simplifying graph convolutional networks," in *ICML*, 2019, pp. 6861–6871.
- [57] K. Xu, W. Hu, J. Leskovec, and S. Jegelka, "How powerful are graph neural networks?" *arXiv preprint arXiv:1810.00826*, 2018.
- [58] D. Lao, X. Yang, Q. Wu, and J. Yan, "Variational inference for training graph neural networks in low-data regime through joint structure-label estimation," in *KDD*, 2022, pp. 824–834.
- [59] T. N. Kipf and M. Welling, "Semi-supervised classification with graph convolutional networks," *arXiv preprint arXiv:1609.02907*, 2016.